REVIEW ARTICLE

Estimation of crustal discontinuities from reflected seismic waves recorded at Shillong and Mikir Hills Plateau, Northeast India

Saurabh Baruah · Dipok K. Bora · Rajib Biswas

Abstract In this study, an attempt is made to determine seismic velocity structure of the crust and upper mantle beneath the Shillong-Mikir Hills Plateau in northeast India region. The principle of the technique is to relate seismic travel times with crustal thickness above the Conrad and Moho discontinuities. Broadband digital waveforms of the local earthquakes make a precise detection of the seismic phases possible that are reflected at these discontinuities. The results show that the Conrad discontinuity is at 18–20 (±0.5) km beneath the Shillong-Mikir Hills Plateau and the Moho discontinuity is at 30 ± 1.0 km beneath the Shillong Plateau and at 35 ± 1.0 km beneath the Mikir Hills.

Keywords Conrad and Moho discontinuities · Reflected seismic waves · Shillong and Mikir Hills Plateau · Travel time

Introduction

The Shillong-Mikir Plateau (SMP) in the northeast region (NER) of India, latitude (25 to 28°N) and longitude (89 to 94°E), is seismically one of the most active zones in the world where 16 large ($M \geq 7.0$) earthquakes and one great $M_S = 8.7$ earthquake of June 12, 1897 (Oldham 1899) occurred during the last ~110 years since 1897. The 1897 great Shillong earthquake caused extensive destruction in the region killing about 1,540 lives with a property loss of $30 million (Tillottson 1953). The region lies in the seismic zone V of India (BMTPC 2003). The zone V is the maximum rating zone in the national seismic zoning map of India. The SMP is part of the Indian shield, which is separated out from the peninsular shield, and moved to the east by about 300 km along the Dauki fault (Evans 1964). The gigantic E–W trending Dauki fault separates the plateau to the north and the Bengal basin to the south (Kayal 2001; Fig. 1). The mighty river Brahmaputra, on the other hand, separates the plateau from the Himalaya to the north. The E–W segment of the river at the northern boundary of the plateau is named Brahmaputra fault (Nandy 2001). The Mikir massif, a part of the Shillong massif, moved to the northeast along the ~300 km long NW–SE trending Kopili fault (Baruah et al. 1997; Nandy 2001; Kayal 2001).

Several hundred earthquakes ($M > 4.0$) are recorded during the past few decades in the region. In addition to the national network run by the India Meteorological Department (IMD), the North-East Institute of Science and Technology-Jorhat (NEIST-J), the National Geophysical Research Institute, Hyderabad (NGRI-H) and several universities established analog networks since 1982. These stations are now upgraded to broadband digital stations with global positioning system (GPS) timing since 2001.

Many authors (e.g., De and Kayal 1990; Mukhopadhyay et al. 1995; Gupta et al. 1984; Kayal and Zhao 1998; Rai et al. 1999; Baruah 1995; Sitaram et al. 2001) have studied the crustal structure in the region using the analog data recorded before 2001. With the recent broadband waveform data, the Moho discontinuity is studied by receiver function analysis (Kumar et al. 2004; Mitra et al. 2005; Ramesh et al. 2005). They infer a gentle dipping Moho reaching a depth of 48 km to the north of SMP. Based on gravity and seismological data, Nayak et al. (2008) suggest

S. Baruah (✉) · D. K. Bora · R. Biswas
Geoscience Division, North-East Institute of Science
and Technology (formerly Regional Research Laboratory),
under Council of Scientific and Industrial Research,
Jorhat, Assam 785006, India
e-mail: saurabhb_23@yahoo.com

Fig. 1 *Map* showing the major tectonic features of the study region. The Great earthquakes of 12 June, 1897 is shown by a *larger red star*. The *red circles* represent the epicenters of the selected earthquakes. To the right, different magnitude ranges of the epicenters are defined: $M_D(A)$ is the average duration magnitude. The digital broadband seismic stations are shown by *green triangles*. The major tectonic features such as the Dauki Fault, Dhubri Fault, Kopili Fault, Oldham Fault, Main Central Thrust and Main Boundary Thrust are also indicated. Each station is numbered as in Table 1; *Inset* map of India indicating the study region. Alongside the depth section plots of the epicenters of the earthquakes used in this study
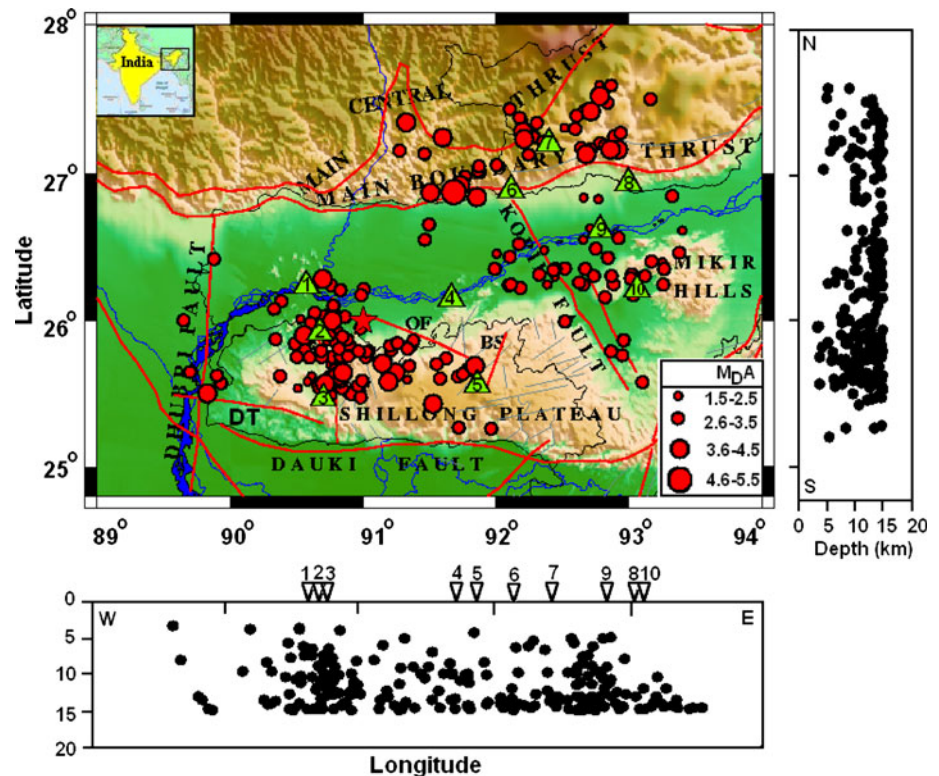
that the Moho beneath the Shillong Plateau is at shallower depth of about 35 km.

No study is, however, made to estimate the Conrad and Moho discontinuities using reflected phases of the local earthquakes recorded by the broadband network in the region. Picking up or precise reading of reflected phases in the analog records of earlier seismic network was difficult. With the advent of digital seismic network, precise detection of reflected phases, however, it is possible to estimate the crustal discontinuities (e.g., Sanford and Long 1965; Mizoue 1971; Sanford et al. 1973; Rinehart and Sanford, 1981; Mizoue and Isao Nakamura 1982; Nakajima et al. 2002). In the present study, we have utilized the broadband seismic waveforms of the local earthquakes to estimate depths of the Conrad and Moho discontinuities. This has been done by estimating travel times of the reflected seismic waves. Results of this study are highlighted here and shed new light on the crustal structure beneath the SMP.

Tectonic setting

The NER India comprises distinct geological units, like the Himalayan frontal arc to the north, the highly folded Indo-Burma mountain ranges to the east, the Brahmaputra alluvium in the Assam valley and the Shillong-Mikir massif between these two arcs, and thick sediments of the Bengal basin to the south (Fig. 1). Seismotectonics of the

region has been the subject of several studies (e.g., Tapponnier et al. 1982; Kayal and De 1991; Kayal 1996, 2001; Angelier and Baruah 2009; Nandy 2001). Bilham and England (2001), based on geodetic and GPS data, proposed a 'pop-up' tectonic model of the Shillong Plateau, and argued that the 1897 great earthquake was produced by a south dipping hidden fault at the northern boundary of the Shillong Plateau; they named it as the 'Oldham fault' that extends from a depth of about 9 km down to 45 km. They further suggested that the Shillong plateau earthquakes are caused by the 'pop-up' tectonics between the Dauki fault and the Oldham fault (Fig. 1). Recent seismicity and tectonics of the region have been reviewed by Kayal et al. (2006); Kayal (2008); Rajendran et al. (2004); Baruah and Hazarika (2008). Prominent geological units of the NER, however, remain geophysically less studied due to inaccessibility of the terrain.

Data analysis and results

Data

We selected 177 best located local earthquakes recorded during 2001–2008 by the broadband seismic network (NEIST-J and NGRI-H) in the region (Fig. 1). These events are recorded with higher signal-to-noise ratio and have clear direct and reflected phases. In addition to the

NEIST-J and NGRI-H network data, the data of the IMD, Gauhati University, Manipur University and Mizoram University are incorporated for precise determination of hypocentral parameters. All broadband seismic stations are operated both in continuous mode and trigger mode, and the seismograms are recorded at 100 samples per second. The recorded seismograms have been corrected by using instrument response based on the eloctrodynamic constant, critical damping, natural frequency of seismometers and bit weight of unit gain of each recording unit for all stations. Table 1 shows the digital stations with the abbreviations used. About 230 seismograms are used for the selected 177 events; epicenters and seismic stations are shown in Fig. 1.

Precision of hypocenter determination depends not only on the distribution of the recording stations but also on velocity structure between source and stations, particularly in an area where lateral heterogeneities are extreme (Okada et al. 1970). We have determined the epicenters using the HYPOCENTER location software of Lienert et al. (1986) based on the crustal velocity model of Bhattacharya et al. (2005). Uncertainties involved in the estimates of epicenters show that about 85% of the events are located with an error of 0–2 km in depth and epicenter, and the error in origin times is of the order of 0–0.5 s. The source receiver distance of the selected events ranges from 35 to 120 km. Duration magnitude (M_D) of these events is estimated in the range 1.7–5.2, and focal depth mostly at 3–15 km.

Reflections from the Conrad discontinuity

Prominent phases after the first P- and S- wave arrivals are observed in the seismograms for shallow crustal earthquakes. These phases are interpreted as reflected P (PxP) and reflected S (SxS) waves, respectively, at the Conrad discontinuity. The PxP and SxS phases are detected at the critical distance ranges. Amplitudes of these phases are diagnostic and sometimes even larger than those of the first arrivals, which suggest that these phases are generated at a sharp velocity (or density) boundary. A few examples of seismograms and travel time plots at a station JPA are illustrated in Fig. 2a, b, respectively. The Fig. 2a indicates the sharp reflected phases in all the seismograms with arrival time differences from 5.1 to 7.4 s. Gradual increase in travel time of these phases with distance depicts reliability of the identified phases. These prominent reflected phases are observed only in the seismograms of shallow crustal (depth ≤ 15 km) earthquakes. The SxS reflections are well identified on the horizontal component seismograms rather than vertical one. Particle motions of these later reflected phases (PxP and SxS) arrived at the stations as compressional and as shear waves, respectively. Analytical results of the particle motions of the reflections at a station JPA are exemplified in Fig. 3.

Table 1 Station names along with abbreviations

| No	Station	Abbreviations	Latitude	Longitude	Elevation (m)
1	Jogighopa	JPA	26.239	90.575	42
2	Manikganj	MND	25.924	90.676	40
3	Nangalbibra	NGL	25.472	90.702	330
4	Gauhati University	GAU	26.152	91.667	69
5	Shillong	SHL	25.566	91.859	1,590
6	Bhairabkunda	BKD	26.890	92.115	210
7	Rupa	RUPA	27.203	92.401	1,470
8	Seijusa	SJA	26.938	92.999	150
9	Tezpur	TZR	26.617	92.783	140
10	Dokmok	DMK	26.216	93.062	200
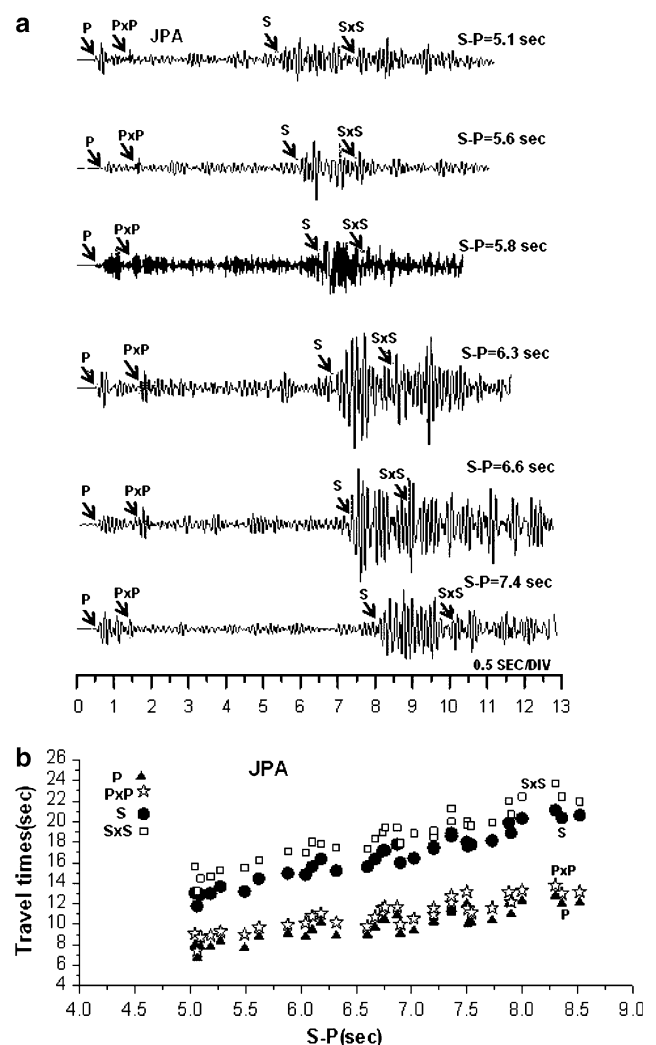
Fig. 2 a Examples of vertical component seismograms recorded at JPA (Jogighopa) station. **b** Plots of travel time versus S–P time for P, PxP, S and SxS phases

Fig. 3 **a** P- and S- wave reflections from the Conrad discontinuity are denoted as PxP and SxS at station JPA (Jogighopa). **b** Particle motion of the P, PxP, S and SxS phases in the *radial* and *vertical plane* are shown
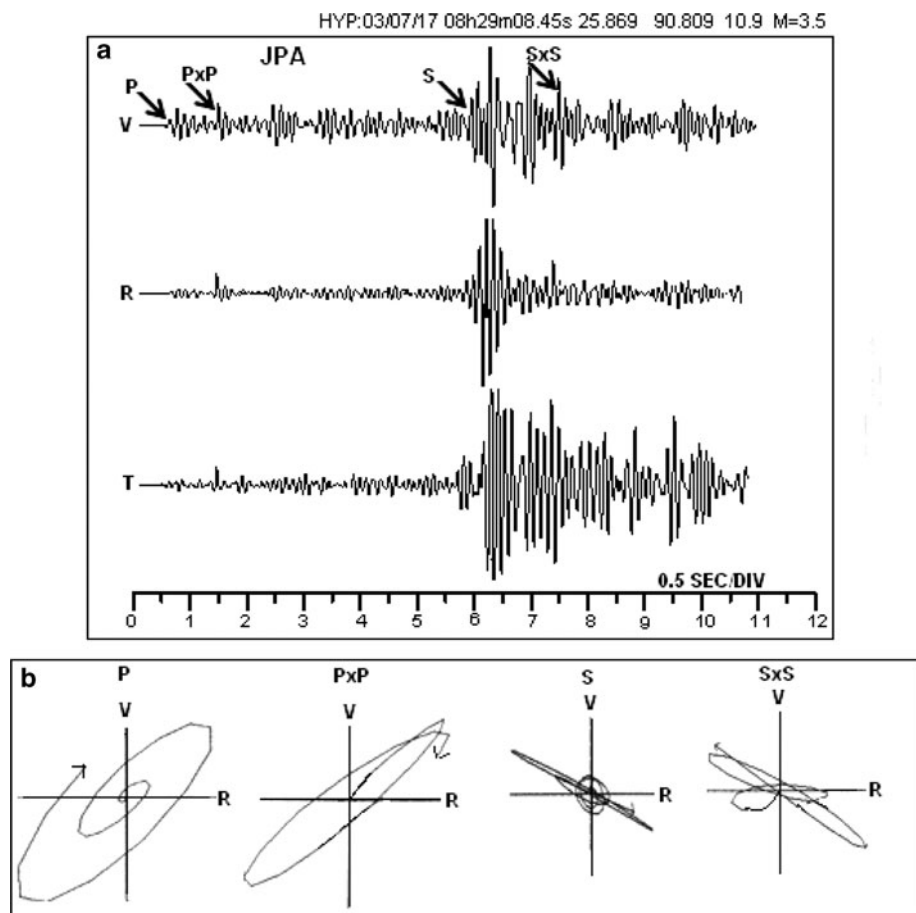
Travel time curves of the PxP and SxS phases are interpreted in terms of depth of the Conrad discontinuity, and the average velocities of the P and S waves in the upper crustal layer are also estimated. Theoretical travel time for a reflected ray from the reflector is calculated by using the relation of Rinehart and Sanford (1981):

$$T = \frac{\sqrt{(2H_1 - h)^2 + \delta^2}}{V} \tag{1}$$

where, H_1 is the depth of the reflector, h is the depth of focus for the event, δ is the epicentral distance and V is the average velocity in the upper crust.

About 48 earthquakes from the Shillong Plateau and 30 earthquakes from the Mikir Hills Plateau are used for the travel time analysis to estimate the Conrad depth. The S–P intervals of the earthquakes are in the range between 4.8 and 8.8 s. The reflected PxP phases from the Conrad discontinuity are observed after 0.6–1.4 s of the first P arrival, and the SxS phases are observed after 1.0–2.6 s of the first S arrival in Shillong Plateau, and 0.7–2.0 s and 1.3–2.8 s in the Mikir Hills Plateau, respectively. The Conrad discontinuity is estimated at a depth of 18 ± 0.5 km beneath the

Shillong Plateau and at 20 ± 0.5 km beneath the Mikir Hills Plateau.

Theoretical travel time curves for both the PxP and SxS reflections from the Conrad discontinuity at a depth (H_1) 18 ± 0.5 km in the Shillong Plateau and at 20 ± 0.5 km in the Mikir Hills Plateau are shown along with the observational data in Fig. 4a, b, respectively. Generally, it is observed that only one combination of (h) and (H_1) produces the theoretical curves that fit the PxP and SxS data equally well. The curves of each reflected phases are given, one for a 3-km depth of focus (h), the other for a 13-km depth of focus. The theoretical curves were computed using the P wave velocity of 5.88 km/s and S wave velocity of 3.53 km/s, respectively, for the Shillong Plateau, and 5.99 km/s and 3.55 km/s for the Mikir Hills Plateau. The theoretical curves envelope both PxP and SxS data (Fig. 4a, b) in about the same way, so that little adjustment is possible in the values of (h) and (H_1). Assuming the V_P and V_S for the lower crustal layer as 6.49 km/s and 3.76 km/s, respectively, for the Shillong Plateau, and 6.84 km/s and 4.0 km/s, respectively, for the Mikir Hills Plateau, the critical distance (Δ_1) and angle of emergence are computed and shown in Table 2.
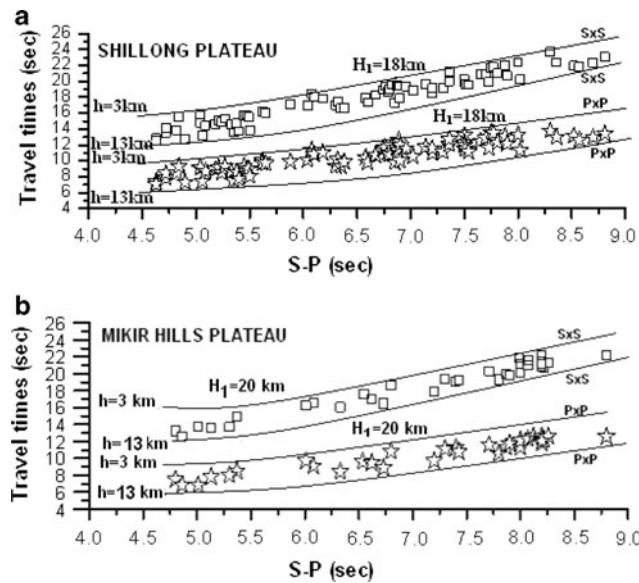
Fig. 4 a and **b** Observed and theoretical travel times of PxP and SxS versus S–P time. Two curves for the reflections at the depth H_1 (*solid lines*) is given, one for the minimum, the other for the maximum depth of earthquake focus h

Table 2 Critical distance and angle of emergence

Observations	Critical distance (km) Δ_1	Angle of emergence (degree)
Shillong Plateau	70.62 km for $h = 3$ km	64.95°
	49.22 km for $h = 13$ km	
Mikir Hills Plateau	66.97 km for $h = 3$ km	61.13°
	47.06 km for $h = 14$ km	

Reflections from the Moho discontinuity

We have analyzed the reflected P (PmP) and reflected S (SmS) waves at the Moho discontinuity, and used their travel times for estimation of the Moho depth. These reflected PmP phases are observed at a time interval of 0.8–2.2 s after the first P arrival and the SmS phases at a time interval of 1.5–3.2 s after the first S arrival in the Shillong Plateau. The respective time intervals are 1.4–2.3 s and 1.9–3.5 s in the Mikir Hills Plateau. These phases are observed at an epicentral distance 75–120 km in both the plateaus for the shallow crustal earthquakes (depth $\leq$ 15 km) only. Amplitudes of these phases are diagnostic, and sometimes larger than those of the first arrivals, which suggest that the phases are generated at a sharp velocity or density discontinuity. A few examples of the seismograms and travel time plots at a station TZR are illustrated in Fig. 5a, b, respectively. An example of the analysis of the particle motions of the reflections from the Moho discontinuity is shown in Fig. 6. About 50 earthquakes in the Shillong Plateau and 70

in the Mikir Hills Plateau are used. Particle motions of these phases are compatible with the compressional and shear waves, respectively (Fig. 6).

Depth of the Moho discontinuity is estimated by using the travel time (T) and epicentral distance (Δ) relation of Mizoue (1971):

$$T = \frac{2H_1 - h}{V_1 \cos i_1} + \frac{2H_2}{V_2 \cos i_2} \qquad (2)$$

$$\Delta = (2H_1 - h)\tan i_1 + 2H_2 \tan i_2 \qquad (3)$$

and

$$\frac{\sin i_1}{V_1} = \frac{\sin i_2}{V_2} \qquad (4)$$

where, V_1 and V_2 denote the velocities in the upper and lower layers of the Earth's crust with thickness of H_1 and H_2, respectively. Let i_1 and i_2 be the incident angles of a seismic ray at the interfaces at a depth of H_1 and H_2, respectively. Then we obtain a theoretical travel time curve for the reflected waves from the Moho discontinuity for a given crustal model assuming a focal depth h less than H_1.

As mentioned earlier, the upper crustal P-wave velocity (V_{P1}) 5.88 km/s and S-wave velocity (V_{S1}) 3.53 km/s in the Shillong Plateau and 5.99 km/s and 3.55 km/s in the Mikir Hills Plateau are considered. The estimated depths of the Conrad discontinuity 18 ± 0.5 km in the Shillong Plateau and 20 ± 0.5 km in the Mikir Hills area are used. The time–distance relations are calculated considering $H_1 = 20 \pm 0.5$ km, since a seismic ray is reflected from the Moho discontinuity in the Mikir Hills area pertaining to the earthquakes being used in this study. After this evaluation, the combination of (H_2) and (h) values will intend to produce a theoretical travel time curve which is fitted to the PmP and SmS data equally well when assuming the most probable velocity values of (V_2) designated as (V_{P2}) for the P waves and (V_{S2}) for the S wave.

The theoretical travel time curves for the PmP and SmS reflections with $H_2 = 15$ km, $V_{P2} = 6.84$ km/s and $V_{S2} = 4.0$ km/s in the Mikir Hills area are drawn in Fig. 7. Similarly, the theoretical travel time curves for the PmP and SmS reflections in the case of $H_2 = 12$ km, $V_{P2} = 6.49$ km/s and $V_{S2} = 3.76$ km/s in the Shillong Plateau area are depicted in Fig. 8. In both plateaus, two curves for each reflected phases are given, for $h = 3$ km as well as for $h = 15$ km corresponding to the upper and lower limits of the focal depths of the earthquakes used. It is observed that the theoretical curves envelope the observed data (Figs. 7, 8). The critical distance (Δ_C), at which the reflected phases are generated, is estimated by the following relation (Telford et al. 1990):

Fig. 5 a Examples of vertical component seismograms with PmP and SmS recorded at TZR (Tezpur) station. **b** Plot of the travel times versus epicentral distance for P, PmP, S and SmS
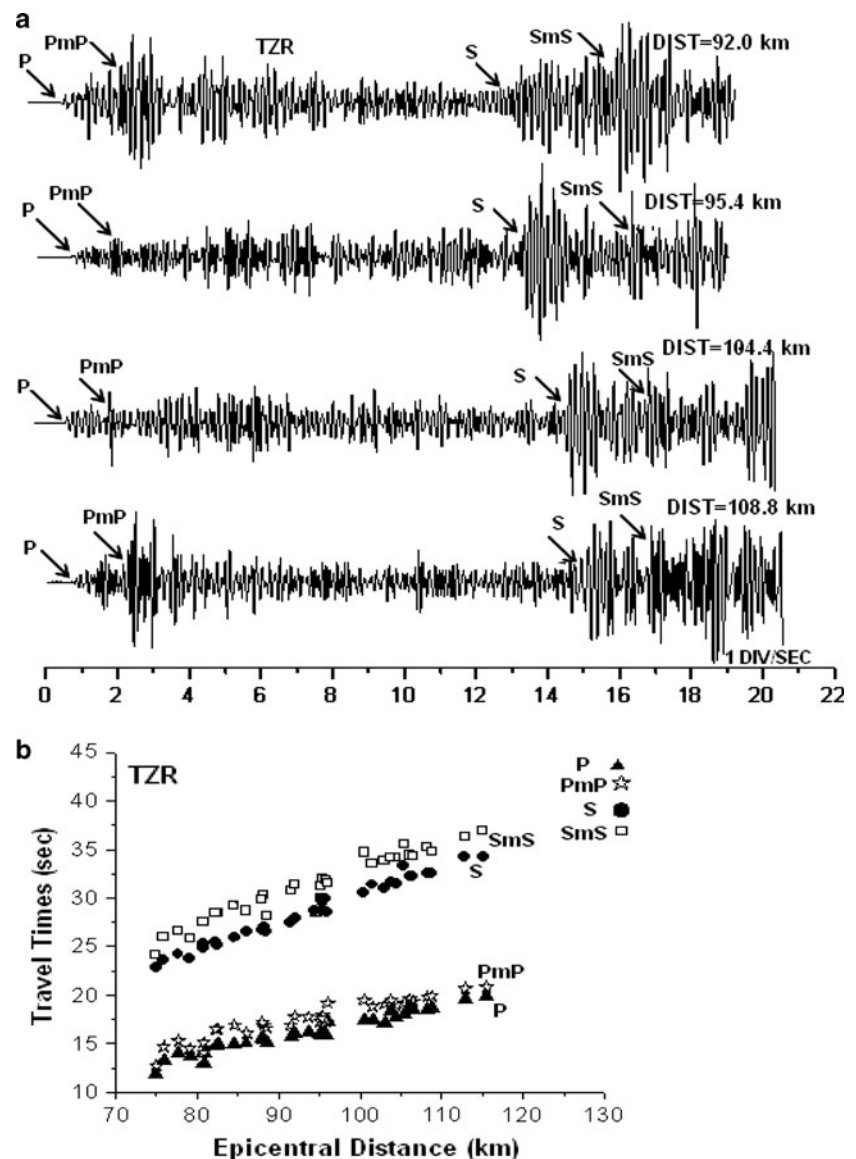
$$\Delta_c = (2H - h)\frac{V_1/V_2}{(1 - V_1^2/V_2^2)^2} \tag{5}$$

where H is the depth of the Moho, h is the focal depth, V_1 and V_2 are the velocities of the upper and lower layer of the Earth's crust, respectively. The estimated depths of H_1 (18 ± 0.5 km) and H_2 (12 ± 0.5 km) beneath the Shillong Plateau, and H_1 (20 ± 0.5 km) and H_2 (15 ± 0.5 km) below Mikir Hills Plateau allow to estimate the critical distances (Δ_2) for reflections at the Moho discontinuity; these are 69.6 and 76.8 km, respectively. In this estimation, we assumed the Pn (V_{P3}) velocity 7.34 and 7.70 km/s for Shillong and Mikir Hills Plateau, respectively. The corresponding angle of emergence is 53.24° in the Shillong Plateau and 50.07° in the Mikir Hills Plateau.

Discussion

The crustal reflections (PxP, SxS, PmP and SmS) are investigated to estimate crustal thickness beneath the SMP. It is observed that the Shillong Plateau earthquakes with S–P interval of 4.8–8.8 s produce two sharp phases; one follows the direct P phase after 0.6–1.4 s, and the other follows the direct S phase after 1.0–2.6 s. Similarly, the events of S–P interval 4.8–8.8 s at the Mikir Hills stations produce two sharp arrivals, one follows the direct P phase after 0.7–2.0 s and the other follows the direct S after 1.3–2.8 s. These phases are identified as the PxP and SxS from the Conrad discontinuity. Further, it is observed that the reflections of the P and S phases, PmP and SmS, respectively, from the Moho discontinuity follow the direct P

Fig. 6 a The P- and S-wave reflections from the Moho discontinuity are denoted as PmP and SmS. **b** Particle motions of the P, PmP, S and SmS phases in the *radial* and *vertical plane* are shown
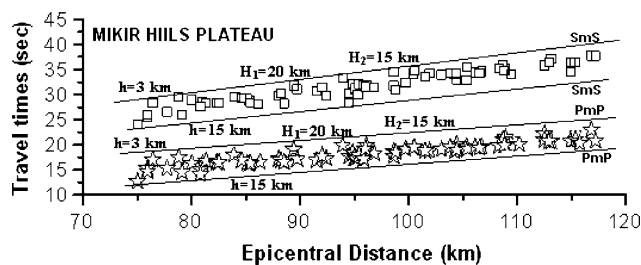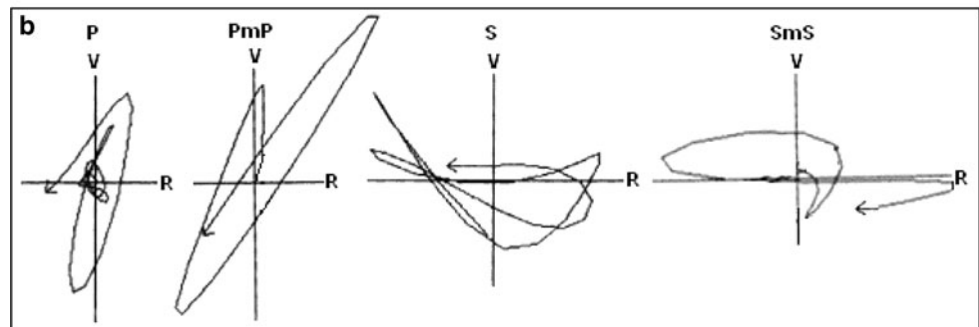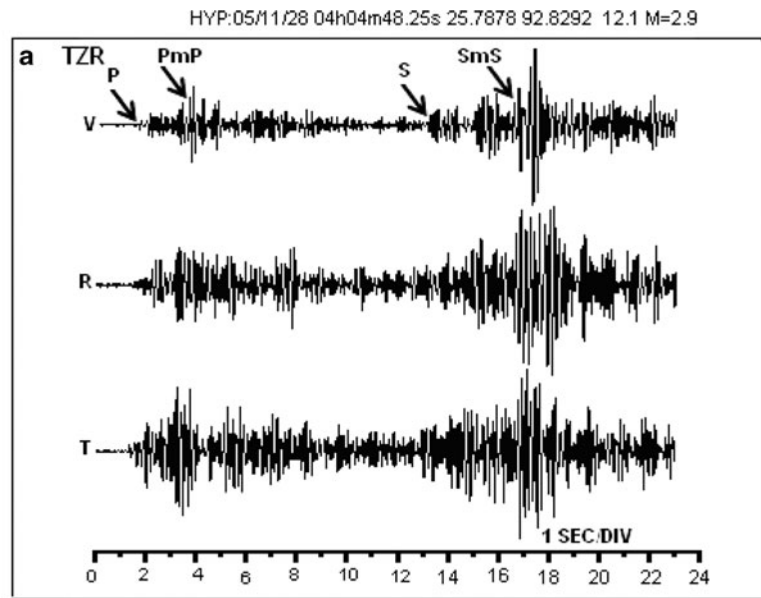

Fig. 7 Observed and theoretical travel times of PmP and SmS versus epicentral distances. Two curves for the reflections from the Moho discontinuity (*solid lines*) are given, one for the minimum and the other for the maximum depth of earthquake focus *h*
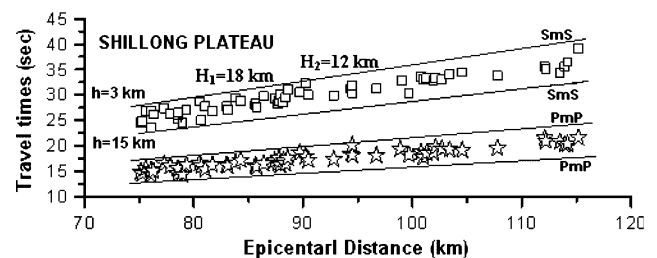
Fig. 8 Observed and theoretical travel times of PmP and SmS versus epicentral distance. Two curves for the reflections from the Moho discontinuity (*solid lines*) are given, one for the minimum and the other for the maximum depth of earthquake focus *h*

after 0.8–2.2 s and the direct S after 1.5–3.2 s, respectively, in the Shillong Plateau. In the Mikir Hills, these phases follow the direct P-wave after 1.4–2.3 s and the direct S wave after 1.9–3.5 s. These prominent phases are observed at an epicentral distance of about 75–120 km in both the Shillong Plateau and Mikir Hills Plateau.

The time–distance relations for the PxP and SxS reflections estimate the Conrad discontinuity at 18 ± 0.5 km depth in the Shillong Plateau and at 20 ± 0.5 km depth in the Mikir Hills Plateau. The depth of the Moho discontinuity is

estimated using the PmP and SmS; it is at 30 ± 1.0 km in the Shillong Plateau and 35 ± 1.0 km in the Mikir Hills Plateau. The crustal model obtained in the present study is shown in Figs. 9 and 10. The critical distance and the angle of emergence in this case are 59.9 km and 64.9° and 57.9 km and 61.1° for the Conrad reflections in the Shillong and Mikir Hills Plateau, respectively. Similarly, the critical distance and the angle of emergence for Moho reflections at the Shillong and Mikir Hills Plateau are 69.6 km and 53.2° and 76.8 km and 50.1°, respectively. It is suggested that there are
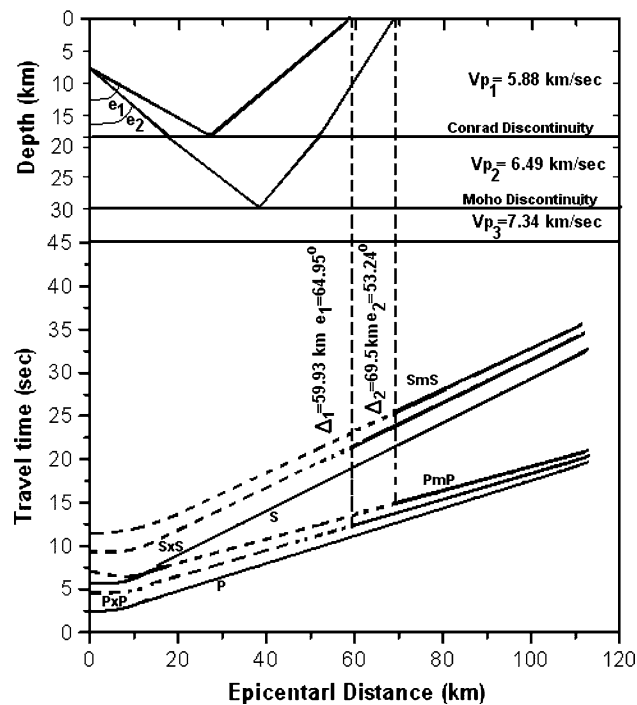
Fig. 9 Travel time curves of the crustal model, Shillong Plateau. Δ_1 = critical distance for the Conrad reflection, e_1 = Critical emergent angle for the Conrad reflections, Δ_2 = critical distance for the Moho reflections, e_2 = critical emergent angle for the Moho reflections

Fig. 10 Travel time curves of the crustal model, Mikir Hills. Δ_1 = critical distance for the Conrad reflections, e_1 = critical emergent angle for the Conrad reflections, Δ_2 = critical distance for the Moho reflections, e_2 = Critical emergent angle for the Moho reflections

significant lateral as well as depth variations of the velocity structure beneath the study region. The complexity arises not only due to the geologic setting but also due to the complex regional tectonic stresses, a N–S stress from the collision zone at the Himalayan arc and an E–W stress from the subduction zone at the Burmese arc (Kayal 1996; 2001).

Several investigations have been made to estimate crustal thickness and 1-D velocity structure in the area using time–distance plot (e.g. Kayal and De 1987 and De and Kayal 1990). The velocity structure for the upper and middle crust of the western Shillong massif indicates P and S wave velocities of 5.9 ± 0.2 and 3.4 ± 0.1 km/s (Mukhopadhyay et al. 1997). These values are in conformity with the velocity model obtained in this study. 3D velocity structure has also been studied by local earthquake tomography (LET) in the area (e.g. Kayal and Zhao 1998; Bhattacharya et al. 2008). These studies have revealed a reasonable velocity model and crustal heterogeneities for improving earthquake locations. All these studies were based on first arrival of P and S wave data of the analog networks operated before 2001. The digital seismograms, recorded by the recent upgraded broadband network since 2001, are fruitfully utilized to identify the reflected phases, and this study enabled us to estimate the Conrad discontinuity as well as the Moho discontinuity with a fair degree of precision. The Conrad discontinuity in the crust has been
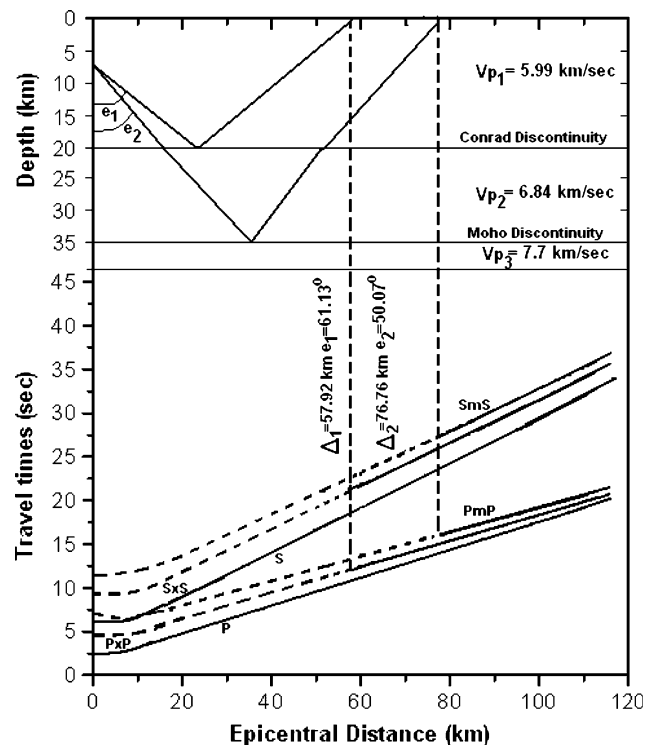
reported by several investigators in some parts of the world (e.g., Mizoue 1971; Horiuchi et al. 1982; Zhao et al. 1990, 1992) but unlike the Moho discontinuity, the Conrad discontinuity is not a diagnostic sharp discontinuity everywhere. In south and central India, several DSS (deep seismic sounding) surveys have been carried out, and the results show 2D velocity structure with a diagnostic Moho discontinuity along all the profiles but the sharp Conrad discontinuity only at places are reported (Kaila and Sain 1997). In our investigation, the broadband seismograms of the local shallow crustal earthquakes have been very useful to identify the sharp Conrad discontinuity.

In a recent teleseismic receiver function analysis with the broadband seismograms, the Moho depth beneath the Shillong Plateau has been estimated by Mitra et al. (2005) and Kumar et al. (2004). The Moho depth is also estimated by gravity modeling, constraining the model with the well-located hypocenters (Nayak et al. 2008). Their investigations estimate the Moho depth at ∼30 km beneath the Shillong Plateau, which is in good agreement with our study. Further, Kumar et al. (2004) reported the presence of Moho interface in the Mikir Plateau at 35 ± 3 km below the Tezpur (TZR) station and at 34 ± 4 km below the Dokmok (DMK) station. Their results are also in good agreement with our study.

Conclusion

We estimated the Conrad and the Moho depths beneath the SMP using the travel times of direct and reflected phases from 177 shallow (depth $\leq$ 15 km) crustal earthquakes. The PmP and SmS phases are critically observed at an epicentral distance of about 75–120 km. It is found that only one combination of focal depth h and crustal depth H reproduces the theoretical curves that match the observed travel time data of the reflected phases. The estimated Conrad depth is 18 ± 0.5–20 ± 0.5 km and Moho depth is 30 ± 1.0–35 ± 1.0 km in the study region. The Moho depth observed in this study is in good agreement with the previous receiver function and gravity studies. The Conrad discontinuity in the SMP is first reported in this study based on reflected phases observed in the broadband seismograms. For Conrad discontinuity, the average critical distance and the corresponding angle of emergence are $\sim$60 km and 64° in the Shillong Plateau, and $\sim$58 km and 61° in the Mikir Hills Plateau, respectively. Similarly, the critical distance and angle of emergence for the Moho reflections at the Shillong and Mikir Hills Plateau is $\sim$70 km and 53°, and $\sim$76 km and 50°, respectively.

References

Angelier J, Baruah S (2009) Seismotectonics in North East India: a stress analysis of focal mechanism solutions of earthquakes and its kinematic implications. Geophys J Int 178:303–326

Baruah M (1995) Body waves investigations in Northeast India, Ph.D. thesis, Dibrugarh University, Assam, India

Baruah S, Hazarika D (2008) A GIS based tectonic map of India. Curr Sci 95:176–177

Baruah S, Duarah R, Yadav DK (1997) Pattern of seismicity in Shillong Mikir plateau and the orientation of compressional axis. J Geol Soc Ind 49:533–538

Bhattacharya PM, Pujol J, Mazumdar RK, Kayal JR (2005) Relocation of earthquakes in the Northeast India region using joint Hypocenter determination method. Curr Sci 89(8):1404–1413

Bhattacharya PM, Mukhopadhyay S, Mazumdar RK, Kayal JR (2008) 3-D seismic structure of the northeast India region and its implication for local and regional tectonics. Jour Asian Ear Sci 33:25–41

Bilham R, England P (2001) Plateau "pop-up" in the Great 1897 Assam earthquake. Nature 410:806–809

BMTPC (2003) Vulnerability atlas- 2nd ed; peer group MoH & UPA; seismic zones of India IS: 1983-2002, BIS, GOI, Seismotectonic atlas of India and its environs,GSI, GOI

De R, Kayal JR (1990) Crustal P-wave velocity and velocity-ratio study in northeast India by a microearthquake survey. Pure Appl Geophys 134:93–108

Evans P (1964) Tectonic framework of Assam. J Geol Soc India 5:80–96

Gupta HK, Singh SC, Dutta TK, Saikia MM (1984). Recent investigations of North East seismicity, Proceedings International symposium continental seismicity and earthquake prediction. Go Gongxu and Ma Xing- Yuan Editors. Seismological Press. Beijing, pp 63–71

Horiuchi S, Ishii H, Takagi A (1982) Two-dimensional depth structure of the crust beneath the Tohoku district, the northeastern Japan arc. I. Method and Conrad discontinuity. J Phys Earth 30:47–69

Kaila KL, Sain K (1997) Variation of crustal velocity structure in India as determined from DSS studies and their implications on regional tectonics. J Geol Soc Ind 49:395–407

Kayal JR (1996) Earthquake source process in northeast India: A review. J Himalayan Geol 17:53–69

Kayal JR (2001) Microearthquake activity in some path of the Himalaya and the tectonic model. Tectonophysics 339:331–351

Kayal JR (2008) Microearthquake Seismology and Seismotectonics of South Asia. Springer, pp 420-423

Kayal JR, De R (1987) Pn velocity study using a temporary seismograph network in the Shillong Plateau, northeast India. Bull Seism Soc Am 77:1718–1727

Kayal JR, De R (1991) Microseismicity and tectonic in Northeast India. Bull Seism Soc Am 81:131–138

Kayal JR, Zhao D (1998) Three dimensional seismic structure beneath Shillong Plateau and Assam Valley, northeast India. Bull Seism Soc Am 88:667–676

Kayal JR, Arefiev SS, Baruah S, Hazarika D, Gogoi N, Kumar A, Chowdhury SN, Kalita S (2006) Shillong Plateau Earthquakes in Northeast India region: complex tectonic model. Curr Sci 91:109–114

Kumar MR, Raju PS, Devi EU, Saul J, Ramesh DS (2004) Crustal structure variations in northeast India from converted phases. Geophys Res Lett 31:1–4. doi:10.1029/2004GL020576

Lienert BR, Berg BE, Frazer LN (1986) Hypocenter: an earthquake location method using corrected, scaled and adaptively damped least squares. Bull Seis Soc Am 76:771–783

Mitra S, Pristley K, Bhattacharya A, Gaur VK (2005) Crustal structure and earthquake focal depths beneath northeastern India and southern Tibet. Geophys J Int 160:227–248

Mizoue M (1971) Crustal structure from travel times of reflected and refracted seismic waves recorded at Wakayama micro-earthquake observatory and its substations. Bull Earthq Res Inst 49:33–62

Mizoue M, Nakamura Isao (1982) Mapping of an unusual crustal discontinuity by microearthquake reflections in the earthquake swarm area near Ashio, Northwestern Part of Tochigi Prefecture, Central Japan. Bull Earthq Res Inst 57:653–685

Mukhopadhyay S, Khattri KN, Chander R (1995) Seismic velocity and related elastic parameters of the crust in the Shillong Massif. J Himalayan Geol 6(1):1–8

Mukhopadhyay S, Chander R, Khattri KN (1997) Crustal properties in the epicentral tract of the Great 1897 Assam Earthquake, northeastern India. Tectonophysics 283:311–330

Nakajima J, Matsujawa T, Hasegawa A (2002) Moho depth variation in the central part of northeastern Japan estimated from reflected and converted waves. Phys Earth Planet Int 130:31–47

Nandy DR (2001) Geodynamics of Northeastern India and the adjoining region. ACB publication, Calcutta, p 209

Nayak GK, Rao VK, Rambabu HV, Kayal JR (2008) Pop-up tectonics of the Shillong Plateau in the great 1897 earthquake (Ms 8.7): insight from the gravity in conjunction with the recent seismological results. Tectonics 27:1–8. doi:10.1029/2006TC002027

Okada H, Suzuki S, Asano S (1970) Anomalous understanding structure in the Matsushiro earthquake swarm area as derived from a fan shooting technique. Bull Earthq Res Inst 48:811–833

Oldham RD (1899) Report on the great earthquake of the 12th June 1897, Mem Geol Surv India 29:1–379

Rai SS, Prakasam KS, Agarwal N (1999) Pn wave velocity and Moho geometry in north eastern India. J Earth Sys Sci 108:297–304

Rajendran CP, Rajendran K, Duarah BP, Baruah S, Anil Earnest (2004) Interpreting the style of faulting and paleoseismicity associated with the 1897 Shillong, northeast India, Earthquake : implications for regional tectonism. Tectonics 23:1–12. doi: 10.1029/2003TC001605

Ramesh DS, Kumar MR, Devi EU, Raju PS, Yuan X (2005) Moho geometry and upper mantle images of northeast India. Geophys Res Lett 32:14301–14304. doi:10.1029/2005GL022789

Rinehart EJ, Sanford AR (1981) Upper crustal structure of the Rio Grande rift near Socorro, New Mexico, from inversion of microearthquake S-wave reflections. Bull Seis Soc Am 71(2): 437–450

Sanford AR, Long LT (1965) Microearthquake crustal reflections, Socorro, New Mexico. Bull Seis Soc Am 55:579–586

Sanford AR, Alptekin O, Toppozada TR (1973) Use of reflection phases on microearthquake seismograms to map an unusual discontinuity beneath the Rio Grande Rift. Bull Seis Soc Am 63:2021–2034

Sitaram MVD, Yadav DK, Goswami K (2001) Study on crustal structure beneath Arunachal Himalaya and Assam. J Geol Soc India 58:285–301

Tapponnier P, Peltzer G, Le Dian AY, Armijo R, Cobbold P (1982) Propagating extrusion tectonics in Asia: new insights from simple experiments with plasticine. Geology 10:611–616

Telford WM, Geldart LD, Sheriff RE (1990) Applied geophysics, 2nd edn. Cambridge University Press, Cambridge, p 769

Tillottson E (1953) The great Assam earthquake of 1950, the completion of papers on the Assam Earthquake of August 15, 1950, Compiled by M.B. Ramachandra Rao, pp 94–96

Zhao D, Horiuchi S, Hasegawa A (1990) Three-dimensional seismic velocity structure of the crust and uppermost mantle in the northeastern Japan arc. Tectonophysics 181:135–149

Zhao D, Hasegawa A, Horiuchi S (1992) Tomographic imaging of P-and S-wave velocity structures beneath northeastern Japan. J Geophys Res 97:19909–19928